Electronic Supplementary Information

Construction of In_2O_3 hierarchical microstructure consisting of single crystalline octahedral particles and polycrystalline fibers for detection of low concentration HCHO

Hui Li, Yingzi Wang, Qian Ma*, Shushu Chu, Hang Li, Yi Wang, Ping Yang*

School of Material Science and Engineering, University of Jinan, 250022, Jinan, P. R. China

*To whom correspondence should be addressed.

E-mail: mse_maq@ujn.edu.cn mse_yangp@ujn.edu.cn

Fax: +86-531-87974453, Tel: +86-531-89736225

Experimental Section

Materials

Indium chloride ($InCl_3$) (98 %, Shanghai Macklin Biochemical Co., Ltd), indium nitrate hydrate ($InN_3O_9 \cdot xH_2O$) (99.9 %, Aladdin Industrial Corporation, China), Polyvinylpyrrolidone (PVP, 1 300 000) (Aladdin Industrial Corporation, China), N,N-dimethylformamide (DMF) and Ethanol (Tianjin Fuyu Fine chemical Co., Ltd) were directly used as received.

Prepareation of other In_2O_3 samples

The synthetic process of other In_2O_3 samples was similar to In_2O_3-FO sample procedure except the calcination temperature of 500, 700, and 800 ^oC and samples were named as In_2O_3-500, In_2O_3-700, and In_2O_3-800, respectively.

Characterization

In_2O_3 samples were prepared by Electrostatic spinning machine (FM-1206, Beijing Future Material Sci-tech Co., Ltd). Scanning Electronic Microscopy (SEM) images and Energy Dispersive Spectrometer (EDS) images of samples were characterized by a field-emission scanning electron microscope (QUANTA 250 FEG, FEI, USA). Transmission electron microscopy (TEM/high-resolution TEM (HRTEM), Tecnai F20, FEI) measured TEM/HRTEM images and selected area electron diffraction (SAED) patterns of samples. X-ray photoelectron spectroscopy (XPS, ESCALAB 250), X-ray diffraction (XRD, D8-ADVANCE of Bruker Corporation, CuKα radiation source), a high resolution Raman spectrometer (LabRAM HR Evolution, HORIBA JOBIN YVON SAS), UV-Vis spectrometer (Hitachi U-4100) tested XPS spectra, XRD patterrns, Raman spectra, and UV-Vis diffuse reflectance spectra (DRS), respectively. Specific surface area and pore size distribution of samples were obtained

by a multifunction adsorption instrument (MFA-140, Builder Company, Beijing).

Fabrication and measurement of gas sensors

Fabrication of gas sensors

Samples were slightly ground with several drops of water to form a paste, which were coated on Ag-Pd interdigital electrodes, and then obtaining sensors.

Performance measurement of gas sensors

Sensors were dried naturally and then stabilized at 300 ^{o}C for 30 min. The gas-sensing performances of samples were evaluated by CGS-4TPs (Beijing Elite Tech Co., Ltd, China). Four sensors were placed in a 1.8 L test chamber. Raising to operating temperature and holding sensors steady for 30 min, resistance was obtained in air, which was named Ra. Test chamber was closed and a certain amount of HCHO was injected obtaining resistance in HCHO gas, which was named Rg. The response of gas sensors was defined as Ra/Rg. Relative humidity and temperature of testing environment are 50 % and 25 ^{o}C, respectively. The response and recovery time was defined as the time taken by the sensors to achieve 90 % of the total resistance change.

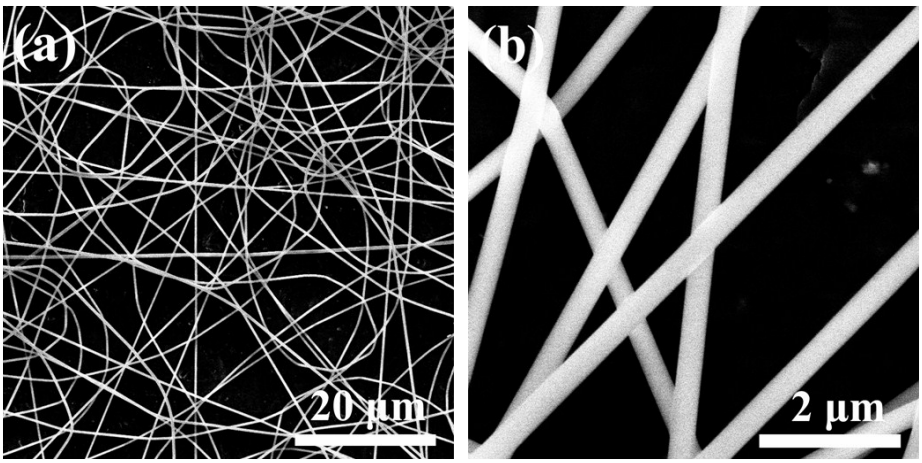

Fig. S1. SEM images of precursor fibers (In_2O_3-FO).

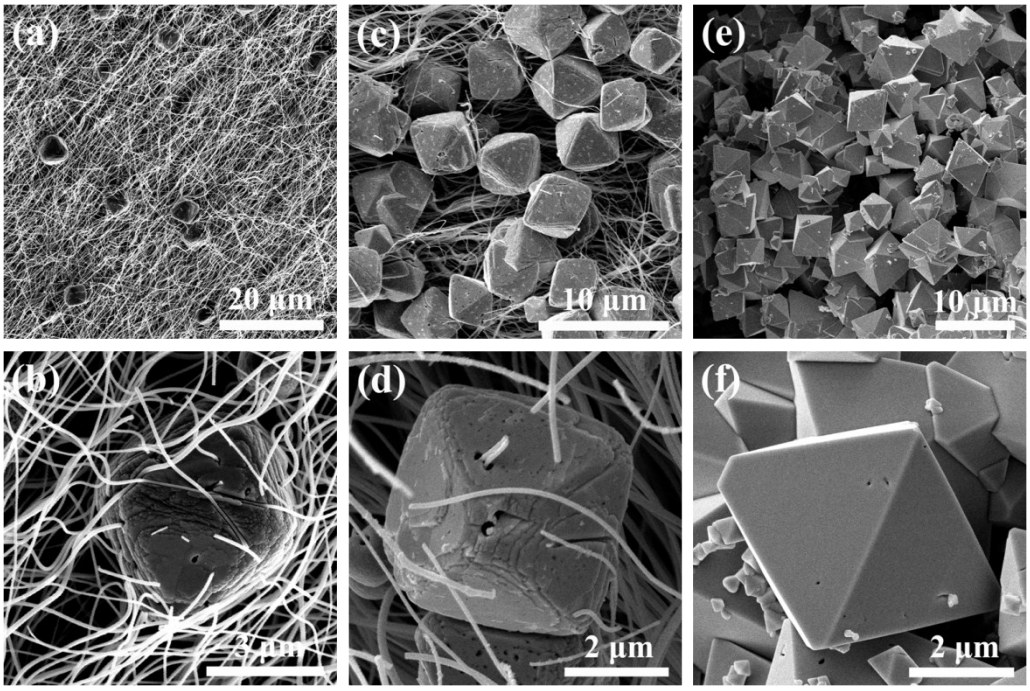

Fig. S2. SEM images of In_2O_3-500 (a,b), In_2O_3-700 (c,d) and In_2O_3-800 (e,f).

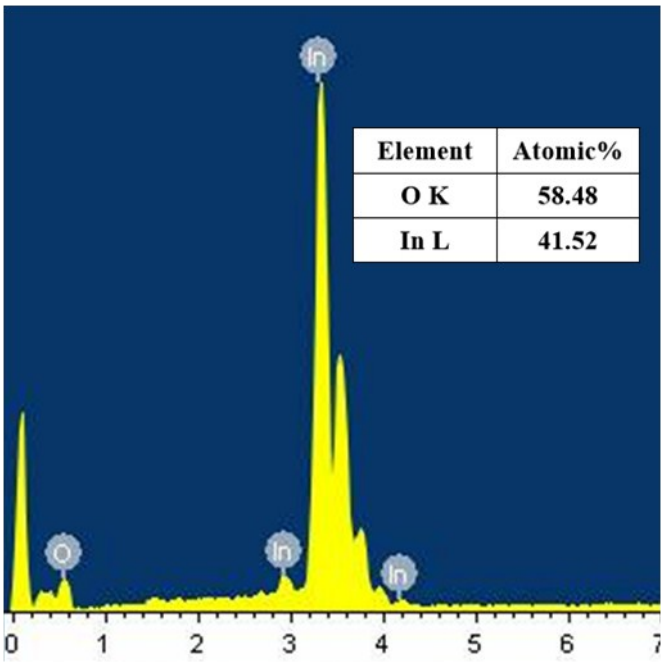

Fig. S3. EDS of In_2O_3-FO.

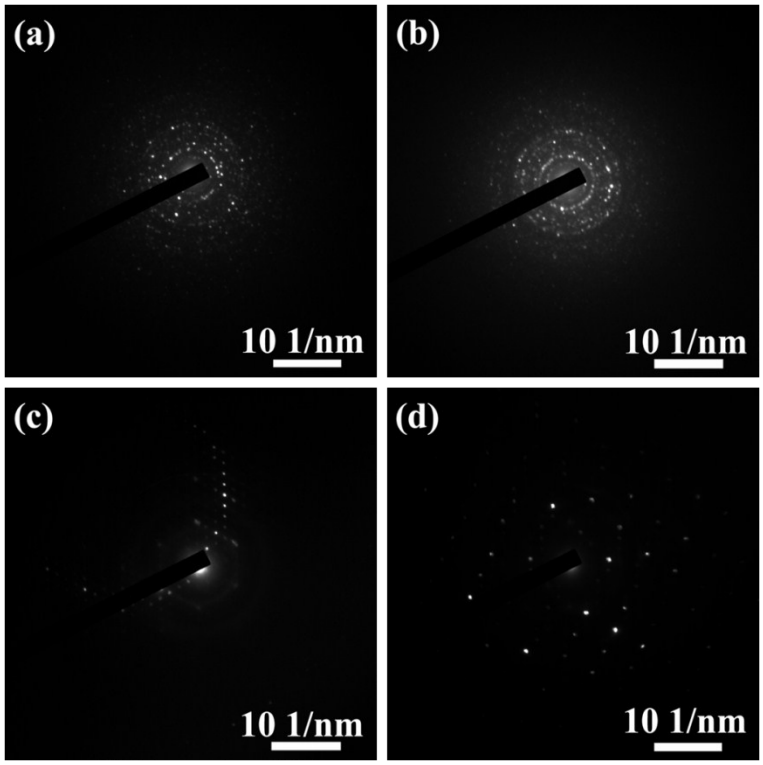

Fig. S4. SAED patterns of samples: (a) In_2O_3-F; (b and c) fiber and octahedral particle of In_2O_3-FO; (c) In_2O_3-O.

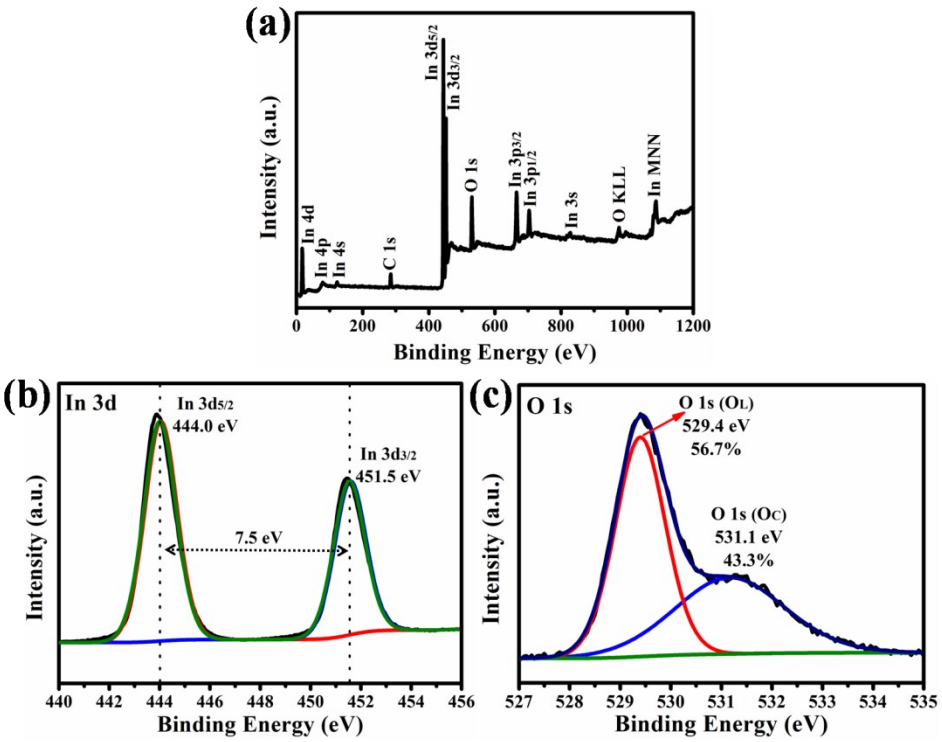

Fig. S5. XPS spectra (a-c) of In_2O_3-FO.

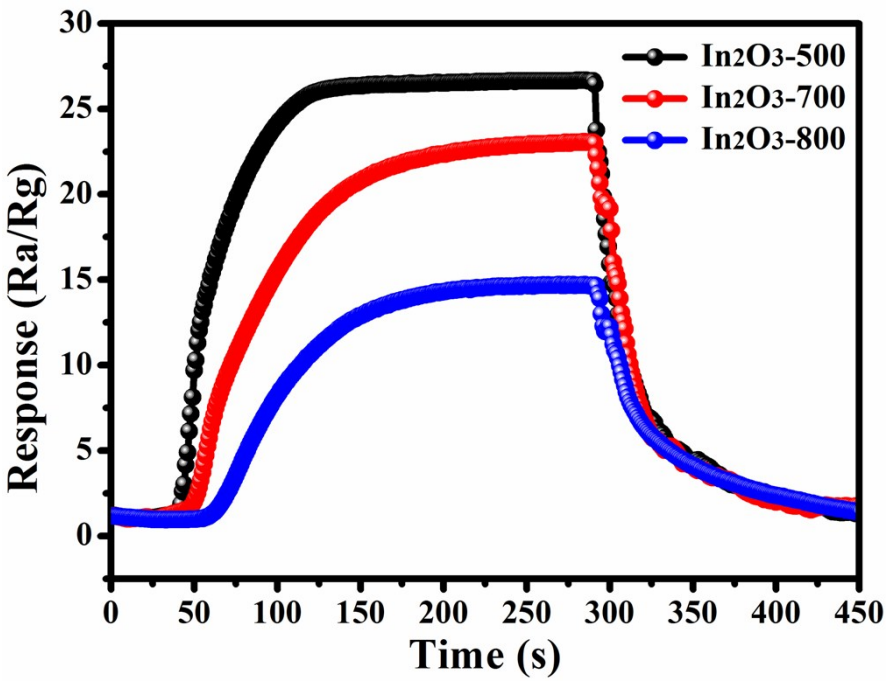

Fig. S6. Response curves of different sensors to 5 ppm HCHO at 160 °C.

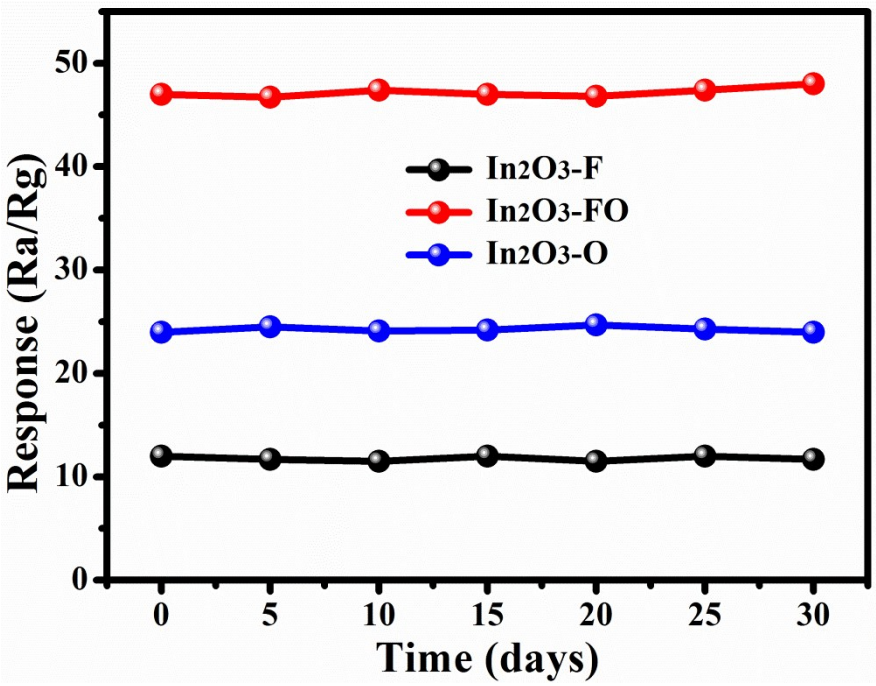

Fig. S7. Long-time stability of samples.

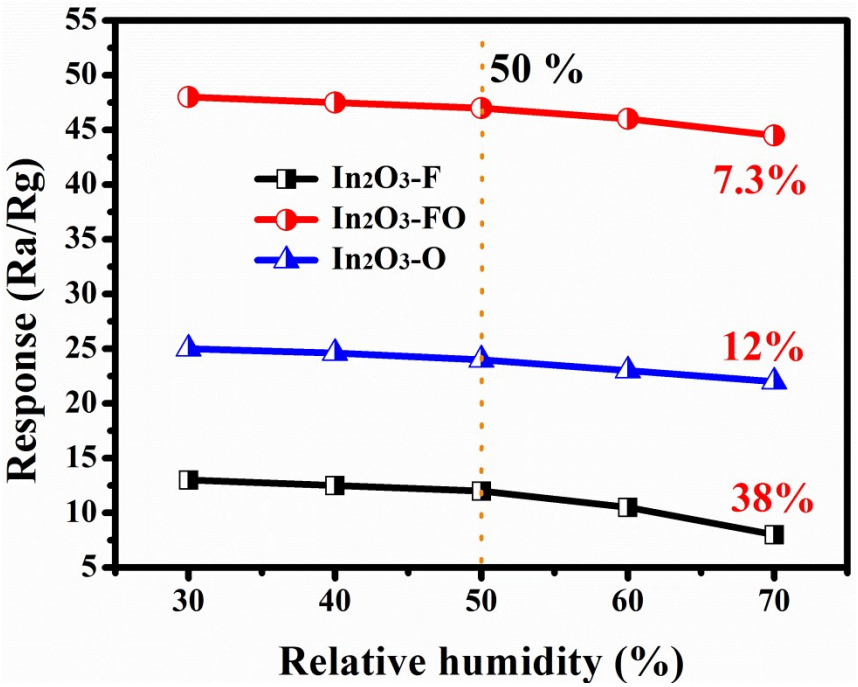

Fig. S8. Responses of samples at different relative humidity.

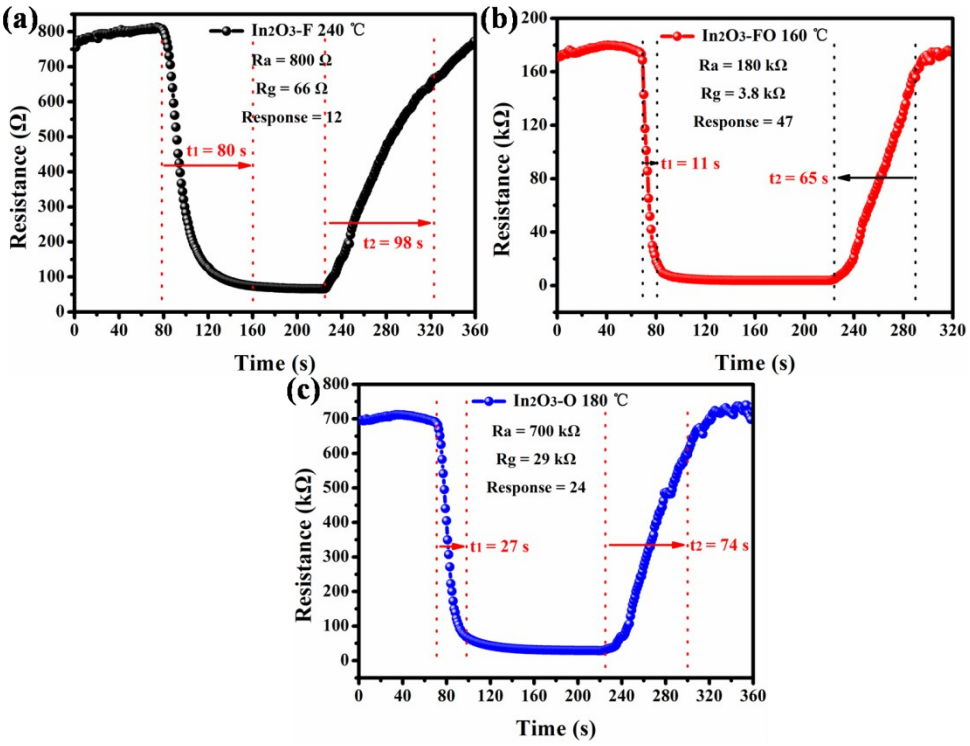

Fig. S9. Response and recovery time curves of sensors to 5 ppm HCHO at optimal operating temperature.

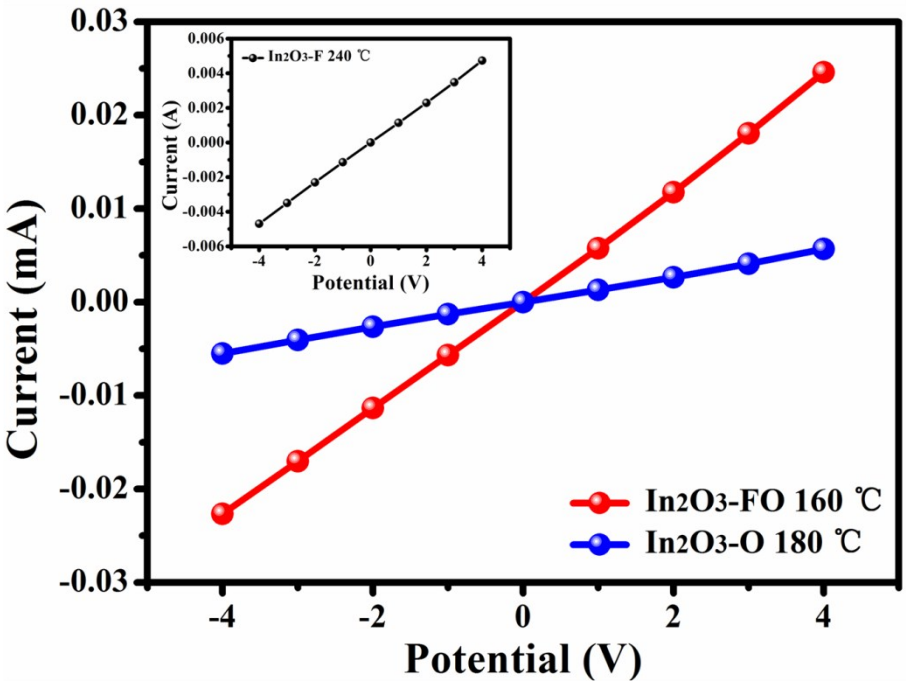

Fig. S10. I-V curves of different sensors within a bias from -4 V to +4 V in air.

Table S1 Comparison of HCHO gas-sensing performances of In_2O_3-based materials.

Material type	HCHO (ppm)	Temperature (ºC)	Response (Ra/Rg)	Response/ Recovery time (s)	Ref.
In_2O_3 hierarchical architectures	100	260	8.6	1/8	S1
Fe-doped In_2O_3 hollow microspheres	50	260	9.43	6/3	S2
Ag-loaded In_2O_3 hierarchical nanostructures	20	240	11.3	0.9/14	S3
In_2O_3 nanoparticles	100	230	80	100/70	S4
WOx clusters decorated In_2O_3 nanosheets	100	170	25	1/67	S5
Ag-functionalized Ni-doped In_2O_3 nanorods	100	160	123.97	1.4/58.2	S6
Co-doped In_2O_3 Nanorods	10	130	23.2	60/120	S7
In_2O_3 hierarchical microstructure	5	160	47	11/65	This work

References

[S1] S. Wang, J. Cao, W. Cui, L. Fan, X. Li and D. Li, *Sensors & Actuators: B. Chemical*, 2018, **255**, 159-165.

[S2] R. Dong, L. Zhang, Z. Zhu, J. Yang, X. Gao and S. Wang, *CrystEngComm*, 2017, **19**, 562-569.

[S3] S. Wang, B. Xiao, T. Yang, P. Wang, C. Xiao, Z. Li, R. Zhao and M. Zhang, *J. Mater. Chem. A*, 2014, **2**, 6598-6604.

[S4] F. Gu, C. Li, D. Han and Z. Wang, *ACS Appl. Mater. Interfaces*, 2018, **10**, 933-942.

[S5] Y. Cao, Y. He, X. Zou and G. D. Li, *Sensors & Actuators: B. Chemical*, 2017, **252**, 232-238.

[S6] X. Zhang, D. Song, Q. Liu, R. Chen, J. Hou, J. Liu, H. Zhang, J. Yu, P. Liu and J. Wang, *J. Mater. Chem. C*, 2019, **7**, 7219-7229.

[S7] Z. Wang, C. Hou, Q. De, F. Gu and D. Han, *ACS Sens.*, 2018, **3**, 468-475.